University of Groningen

The flexural stiffness of superficial neuromasts in the zebrafish (Danio rerio) lateral line

McHenry, Matthew J.; van Netten, Sietse M.

IMPORTANT NOTE: You are advised to consult the publisher's version (publisher's PDF) if you wish to cite from it. Please check the document version below.

Document Version
Publisher's PDF, also known as Version of record

Link to publication in University of Groningen/UMCG research database

The flexural stiffness of superficial neuromasts in the zebrafish (*Danio rerio*) lateral line

Matthew J. McHenry[1],* and Sietse M. van Netten[2]

[1]*Department of Ecology and Evolution, 321 Steinhaus Hall, University of California, Irvine, CA 92697, USA and*
[2]*Department of Neurobiophysics, University of Groningen, Neurobiophysics, Nijenborgh 4, 9747 AG Groningen, The Netherlands*

*Author for correspondence (e-mail: mmchenry@uci.edu)

Summary

Superficial neuromasts are structures that detect water flow on the surface of the body of fish and amphibians. As a component of the lateral line system, these receptors are distributed along the body, where they sense flow patterns that mediate a wide variety of behaviors. Their ability to detect flow is governed by their structural properties, yet the micromechanics of superficial neuromasts are not well understood. The aim of this study was to examine these mechanics in zebrafish (*Danio rerio*) larvae by measuring the flexural stiffness of individual neuromasts. Each neuromast possesses a gelatinous cupula that is anchored to hair cells by kinocilia. Using quasi-static bending tests of the proximal region of the cupula, we found that flexural stiffness is proportional to the number of hair cells, and consequently the number of kinocilia, within a neuromast. From this relationship, the flexural stiffness of an individual kinocilium was found to be 2.4×10^{-20} N m². Using this value, we estimate that the 11 kinocilia in an average cupula generate more than four-fifths of the total flexural stiffness in the proximal region. The relatively minor contribution of the cupular matrix may be attributed to its highly compliant material composition (Young's modulus of ~21 Pa). The distal tip of the cupula is entirely composed of this material and is consequently predicted to be at least an order of magnitude more flexible than the proximal region. These findings suggest that the transduction of flow by a superficial neuromast depends on structural dynamics that are dominated by the number and height of kinocilia.

Key words: lateral line, fish, mechanosensory, hair cells.

Introduction

The lateral line system of fish and amphibians includes two classes of mechanosensory organ on the surface of the body that function to sense water flow. The signals detected by these organs, called canal and superficial neuromasts, mediate behaviors as disparate as spawning (Satou et al., 1994), obstacle detection (Hassan, 1986) and rheotaxis (Montgomery et al., 1997). Both types of neuromast are mechanically excited by fluid forces that are transduced into receptor potentials by hair cells. The structural properties of a neuromast govern its response to flow, yet only the mechanics of canal neuromasts have been investigated in detail (Kroese and van Netten, 1989; van Netten and Kroese, 1989; van Netten and Kroese, 1987). It is consequently unclear how superficial neuromasts transduce flow or how the components of superficial neuromast morphology affect transduction. Therefore, the aim of this study was to measure the flexural stiffness (i.e. flexural rigidity or bending stiffness) of superficial neuromasts in the interest of understanding the structural basis of flow sensing in these organs.

Although canal and superficial neuromasts are similar in anatomical composition, their morphological distinctions suggest that they function differently. Both types include hair cells with kinocilia that are surrounded by a gelatinous cupula that is exposed to water flow. The pear-shaped hair cell bodies beneath the base of the cupula are surrounded by supporting cells and are innervated by efferent and afferent fibers (Dijkgraaf, 1952). However, the cupulae of superficial neuromasts protrude into the surrounding water (Fig. 1A,B), whereas canal neuromasts are recessed into a channel beneath the scales. The hemispherical cupula within this channel behaves as a rigid body that slides along the epithelium when excited by flow (van Netten and Kroese, 1989; van Netten and Kroese, 1987). In contrast, superficial neuromasts have an elongated cupula (Fig. 1B,C) that bends in flow (Schulze, 1861; Cahn and Shaw, 1962; Dinklo, 2005). Therefore, a superficial neuromast appears to operate as a cantilevered beam with a flexural stiffness that affects how mechanical information is transferred to the mechanosensory hair cells.

Subtle morphological differences in superficial neuromasts are capable of greatly influencing their flexural stiffness. The flexural stiffness is equal to the product (*EI*) of material and structural components (Timoshenko, 1983). Material stiffness, known as Young's modulus (*E*), varies by at least five orders of magnitude among biological materials (Wainwright et al., 1976). The cupular material is composed of a
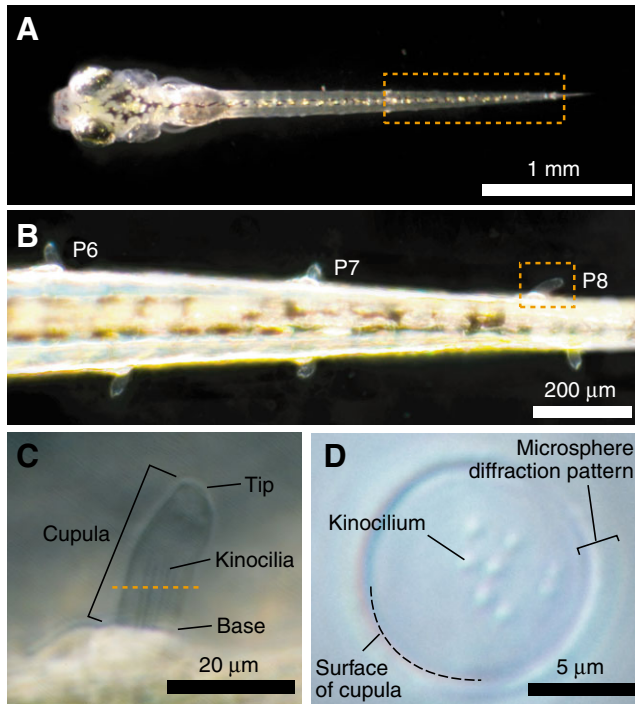
Fig. 1. The morphology of superficial neuromasts in the lateral line of a zebrafish larva. Photographs from separate individuals illustrate the scale and location of the neuromast studied and its constitutent morphology. (A) A larva from a dorsal perspective illustrates the location of the P8 neuromast. The dashed lines show the region of interest in B. (B) The trunk neuromasts are visible in the caudal region with incident illumination. A single P8 neuromast is highlighted by dashed lines. (C) The kinocilia and cupula of a P8 neuromast are visible when examined with Nomarski optics after coating the cupula with polystyrene microspheres. A visual slice parallel to the sagittal plane (dashed line) is shown in D. (D) This cross-section of the cupula illustrates its major morphological features.

potential to relate neuromast dynamics to the biophysics of hair cells because this species is a major model for the study of mechanotransduction (Sidi et al., 2003; Corey et al., 2004). Additionally, an understanding of the mechanics of a superficial neuromast could assist the design of engineered flow sensors (Fan et al., 2002; Peleshanko et al., 2007).

The present study examined the contributions of the kinocilia and the cupular matrix to flexural stiffness by direct measurements. From these measurements and morphometrics, we formulated predictions of flexural stiffness along the height of the cupula. Conducting these experiments on the trunk neuromasts of zebrafish larvae allowed these structures to be visualized with Nomarski optics (Metcalfe et al., 1985) while intact on the body. The morphology of these neuromasts changes little over the course of growth (Webb and Shirey, 2003), as in other species (Munz, 1989). Therefore, our results have the potential to be applicable to the superficial neuromasts of a broad diversity of larval and adult fishes.

Materials and methods

All experiments were conducted on zebrafish (*Danio rerio*, Hamilton 1922) larvae between 5 and 8 days post-fertilization (dpf). All larvae were raised and maintained according to standard protocols (Westerfield, 1995) on a 14 h/10 h light/dark cycle between 26°C and 29°C. Experiments were performed on anesthetized larvae in a perfusion chamber with a solution of embryo media (Brand et al., 2002) containing 0.02% of MS-222 anesthetic (Argent, Redmond, WA, USA). At 5 days of development, the lateral line system is composed entirely of superficial neuromasts (Metcalfe et al., 1985) with hair cells that produce transducer potentials (Nicolson et al., 1998). These cells are innervated by afferent nerves (Alexandre and Ghysen, 1999; Metcalfe et al., 1985), and larvae respond to an impulsive jet of flow with a startle response (Liu and Fetcho, 1999). Therefore, the lateral line system appears to be fully functional by the earliest age at which we ran our experiments.

Morphological measurements

Cupulae were observed with a novel visualization technique (Fig. 1C,D). The trunk of an anesthetized larva was perfused with a solution of polystyrene particles (0.1 μm diameter; Polysciences Inc., Warrington, PA, USA). This particle coating made cupulae visible under polarized or Nomarski optics on a compound microscope (Zeiss Axioskope with ×40 water immersion objective with additional ×3 magnification). We verified that the innermost ring of the diffraction pattern created by these particles corresponds to the location of the cupular surface by touching the cupula with a dull probe. This technique represents an advance in methodology because past approaches for visualizing cupulae have relied on vital stains that either caused shrinkage or provided inconsistent results (Blaxter, 1984).

Digital photographs of cupulae coated with microspheres were used for morphological measurements. Visual cross-sections of cupulae were photographed (2080 pixels× 1542 pixels; Jenoptik, ProgRes C10 plus, Laser Optik Systeme GmbH, Jena, Germany) and these photographs were analyzed with a custom-made program written in Matlab (version 7.2;

glycosaminoglycan gel (Sato, 1962; Thomopolous, 1958) and may therefore have a Young's modulus that is many orders of magnitude lower than that of the kinocilia, which possess rigid microtubles (Flock and Duvall, 1965). The structural component of flexural stiffness is calculated as the second moment of area (*I*) of a beam's cross-section, which varies with the fourth-power of the diameter of a cylindrical beam (Gere, 2001). This relationship suggests that flexural stiffness may vary substantially due to small differences in diameter. For example, a 50% increase in diameter causes the second moment of area, and consequently flexural stiffness, to increase by a factor of 5. Therefore, the flexural stiffness of a superficial neuromast depends strongly on its cross-sectional size and the Young's modulus of the kinocilia and cupular matrix.

The mechanics of superficial neuromasts are relevant to multiple areas of investigation. An understanding of these mechanics would provide a basis for functional interpretations of evolutionary (Northcutt, 1989; Webb, 1989; Webb, 1990) and ontogenetic (Appelbaum and Riehl, 1997; Blaxter and Fuiman, 1989; Poling and Fuiman, 1997; Webb and Shirey, 2003) patterns of variation in lateral line morphology among fishes. Furthermore, research on zebrafish larvae has the

Mathworks, Natick, MA, USA) that measures the position of user-selected coordinates. Cupula diameter was measured at three positions along the height of the cupula (Fig. 1D): at the base of the cupula ($z=0\ \mu m$), approximately mid-height ($z=16\ \mu m$), and at a position near to the distal end ($z=32\ \mu m$). In addition, the number of kinocilia was visually inspected and recorded at $4\ \mu m$ intervals along the height of the cupula.

Measurement of flexural stiffness

The flexural stiffness of individual cupulae was measured in larvae restrained in an agar cast. The agar (low melting point, BP1360-100; Fisher Scientific, Waltham, MA, USA) provided a compliant surface that did not damage larvae, while firmly holding the body. This cast was created by pouring a molten solution (heated to 36°C) of 1% agar and 0.02% MS-222 in embryo media around a glass probe with a diameter that accommodates the width of the head of a larva (~200 μm). Once cooled, the cast was submerged in embryo media (to prevent the introduction of air bubbles) and the probe was removed. Larvae were oriented on their side and pressed into the indentation created by the glass probe. This allowed the lateral surface of the body to be viewed from a fixed-stage compound microscope (Zeiss Axioskope 2FS with ×40 water-immersion objective and ×2.5 magnification cube) with transmitted illumination through the larva's body and the agar cast (Fig. 2A).

Stiffness measurements were based on recordings of the deflection of a glass fiber as it was slowly pressed against the surface of the cupula. Glass fibers of lengths between 6 and 9 mm were cut from cloth tape insulation (Fisher Scientific). Both the glass fiber and the cupula were modeled as cantilever beams with a force applied at a known distance from their clamped bases. This is expressed mathematically by solving the Euler–Bernoulli beam equations for the relationship between force (F) applied at a distance (d) from its base and the deflection (δ) generated at this position, assuming small deflections ($\delta/d<0.1$) (Gere, 2001):

$$F = \frac{3EI\delta}{d^3}\ . \tag{1}$$

In our quasi-static experiments, the force generated by the glass fiber was equal and opposite to the elastic force of the cupula. This is expressed by the following force-balancing relationship:

$$\frac{3(EI)_{cup}\delta_{cup}}{h^3} = \frac{3(EI)_{fiber}\delta_{fiber}}{l^3}\ , \tag{2}$$

where $(EI)_{cup}$, δ_{cup} and h are, respectively, the cupular flexural stiffness, cupular displacement and position of the fiber along the height of the cupula; and $(EI)_{fiber}$, δ_{fiber} and l are, respectively, the flexural stiffness, deflection and length of the glass fiber. The deflection of the fiber was calculated as the difference between the displacement of its base and tip (i.e. $\delta_{fiber}=x_{base}-x_{tip}$), and the deflection of the cupula was equal to the displacement of the fiber tip (i.e. $\delta_{cup}=x_{tip}$). We assumed a linear relationship (see Eqn 2) between the displacement of the fiber's tip and base (i.e. $x_{tip}=mx_{base}$). The slope of this relationship (m) was found by a least-squares linear curve fit of the measured displacement of the tip of the glass fiber (x_{tip}, dependent variable) as a function of the displacement of the base
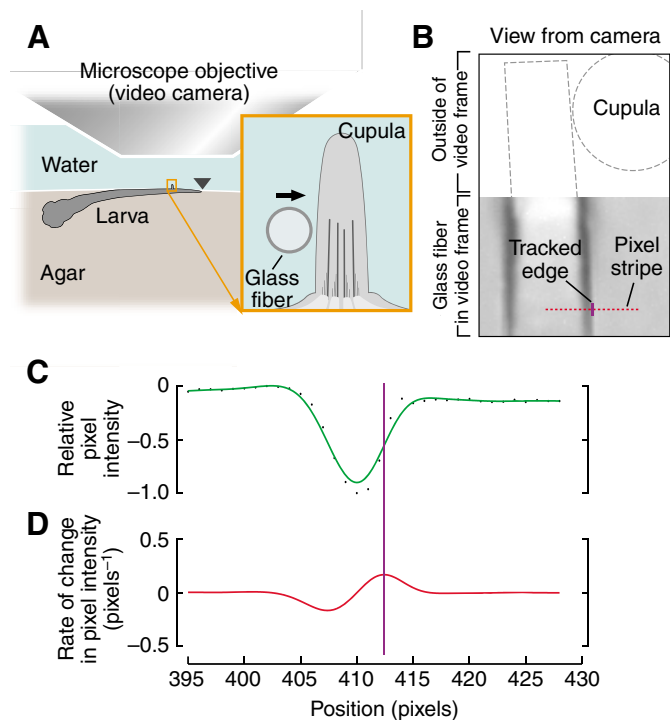

Fig. 2. High-speed microscopy was used to track the position of the glass fiber used for stiffness measurements. (A) Individual larvae were inserted into a bed of agar with their tails pinned beneath a dull probe (triangle) under the objective lens of a fixed-stage compound microscope. When held in this position, the tip of a glass fiber was pressed against the middle of an individual neuromast (inset). (B) During experiments, the position of the fiber was recorded with a high-speed video camera mounted on the microscope. Video recordings were analyzed to track the movement of the edge of the glass fiber. A single video frame from one of these recordings is shown with the edge (purple line) that was found for the prescribed pixel stripe. (C) The pixel intensity along this stripe is shown with a curve fit (green line). (D) The first derivative of the fitted line with respect to position was used to find the position of maximum change in pixel intensity. This point was interpreted as the edge of the glass fiber.

(x_{base}, independent variable). Given that $\delta_{fiber}/\delta_{cup}= (x_{base}-x_{tip})/x_{tip}=(1-m)/m$, Eqn 2 may be rewritten as:

$$(EI)_{cup} = (EI)_{fiber}\left(\frac{h}{l}\right)^3 \frac{1-m}{m}\ . \tag{3}$$

This equation was used to calculate the flexural stiffness of a cupula from measurements of the flexural stiffness of the glass fiber [$(EI)_{fiber}$], its length (l), the position of contact along the cupular height (h) and the slope (m).

Displacement of the base of the glass fiber (x_{base}) was measured with a custom-built device. A high-precision micromanipulator (DS-4F, Newport Corp., Mountain View, CA, USA) was used to translate the base of the glass probe in the direction of loading. This translation was recorded with an optical strain gauge (SPOT-2D, OSI Optoelectronics, Hawthorn, CA, USA) with a custom-built amplifier that provided precision at the 0.01 μm level.

The position of the fiber tip (x_{tip}) was recorded with an optical technique. The compound microscope (described above; see Fig. 2B) was focused near the distal tip of the fiber, but just proximal to its contact with the cupula. A high-speed video camera (1024 pixels $\times$ 1024 pixels, 1000 frames s^{-1}; 1024PCI, Photron USA Inc., San Diego, CA, USA) mounted onto the compound microscope recorded the position of the fiber. We developed a Matlab program to analyze these recordings in order to automatically track the position of the edge of the glass in a video frame (Fig. 2A). This program considered the pixel intensity along a user-defined strip of pixels that spanned the edge of the fiber in a video frame (Fig. 2A). A smoothing spline was fitted to the values of relative pixel intensity along this strip (Fig. 2C). The program defined the edge of the fiber as the point of most rapid positive change in intensity by finding the maximum of the first derivative of the smoothing spline (Fig. 2D). The time history of a position recording was digitally filtered in Matlab with a low-pass Butterworth filter with a cut-off frequency of 1.3 Hz to remove mechanical and electrical noise. This relatively low cut-off was necessary because of low frequency (~2 Hz) interference by air currents around the preparation. However, the signal was not filtered out because loads were applied over durations of about 10 s and the transient period during initial loading was excluded from the analysis.

Glass fibers were calibrated by calculating their flexural stiffness from deflection measurements when loaded with a known weight. Weights small enough to generate deflections of less than 10% were constructed from fine steel wire (76 μm diameter) with a mass below the precision of a conventional fine balance. This was achieved by weighing a relatively heavy length of wire (15 cm) and calculating the ratio of this weight to the length of the wire. Small (1.3–2.8 mm) portions of the wire were then cut and their lengths were measured from digital photographs (Canon 350D with 3456 pixels$\times$2304 pixels on a Zeiss Stemi 2000-C microscope). The product of these lengths and the ratio of the measured weight to length yielded weights ranging between 0.62 and 1.31 μN. The glass fibers were oriented horizontally and wires bent into a 'C' shape were placed near the tip of a fiber. The deflections of fibers under this load were measured by digital photographs and used to calculate their flexural stiffness (with Eqn 1). Fibers had flexural stiffness values ranging from 0.54$\times$10^{-11} to 1.39$\times$10^{-11} N m^{2}.

Error analysis

An error analysis was conducted to assess the major sources of uncertainty in our method of measuring flexural stiffness. For each parameter that was factored into our calculation of stiffness (Eqn 3), we calculated random sources of error as the standard deviation of the mean (SDOM) of repeated measurements. SDOM assumes negligible systematic error and is equal to the standard deviation of the measurements divided by the square root of their sample size (Taylor, 1982). The propagation of these errors in the calculation of flexural stiffness was determined by examining how error in each parameter in Eqn 3 relates to the total error, $\Delta(EI)_{cup}$, in the measurement. This yielded the following relationship for the total proportional error in our measurements (Taylor, 1982):

$$\frac{\Delta(EI)_{cup}}{(EI)_{cup}} = \left[\left(\frac{\Delta(EI)_{fiber}}{(EI)_{fiber}}\right)^2 + \left(\frac{\Delta m}{m(1-m)}\right)^2 + \left(3\frac{\Delta l}{l}\right)^2 + \left(3\frac{\Delta h}{h}\right)^2\right]^{1/2}. \quad (4)$$

Each squared term in this equation expresses the relative contribution of a parameter to uncertainty in our measurement of the flexural stiffness of the cupulae. The following values for these terms were found by repeated measurements: $\Delta(EI)_{fiber}/(EI)_{fiber}$=0.10, $\Delta m/m(1-m)$=0.04, $3\Delta l/l<$0.01, $3\Delta h/h$=0.06. Therefore, error in the calibration of the stiffness of the glass fiber contributed most to the total error in our measurements. The total error calculated from all sources is equal to 0.12 or 12%.

A consideration of the error in our measurements influenced our experimental methodology. The equation for total error (Eqn 4) illustrates how absolute errors in the slope m propagate in proportion to the inverse of $m(1-m)$. This suggests that error due to the slope can be minimized at m=0.5. This slope occurs when the deflections of the glass fiber and cupula are equivalent, which is achieved when the ratio of flexural stiffness to the cube of length for the two structures is equivalent. Such conditions were most easily met by adjusting the length of the glass fiber. However, a number of experiments deviated significantly from m=0.5. We therefore eliminated measurements outside of the 1/8$<m<$7/8 range in order to avoid generating excessively large errors.

Flexural stiffness of kinocilia

Natural variation in the number of hair cells within a neuromast provided the opportunity to examine the effect of kinocilia on the flexural stiffness of the cupula. All stiffness measurements were conducted on neuromasts located in the same caudal region (P8) (Raible and Kruse, 2000), which contained between 5 and 13 kinocilia. By assuming that stiffness varies in proportion to the number of kinocilia, the flexural stiffness of the proximal region of the cupula was predicted to be the sum of the stiffness from the cupular matrix [$(EI)_{matrix}$] and the product of the number of kinocilia (n) and the flexural stiffness of an individual kinocilium [$(EI)_{kino}$]:

$$(EI)_{cup}=n(EI)_{kino}+(EI)_{matrix}. \quad (5)$$

We solved for $(EI)_{kino}$ and $(EI)_{matrix}$ from measurements of $(EI)_{cup}$ by a linear regression with n as the independent variable. For this regression, we calculated the mean values of measurements grouped by the number of hair cells. These values were weighted by sample size in a linear least-squares curve fit (Quinn and Keough, 2002) for the slope [i.e. $(EI)_{kino}$] and intercept [i.e. $(EI)_{matrix}$] of Eqn 5. Young's modulus of the matrix material was calculated by dividing $(EI)_{matrix}$ by the second moment of area for the base of the cupula, I_{cup}. The second moment of area was calculated from a measurement of the diameter of the cupula at its base (D), using the following equation (Gere, 2001):

$$I_{cup} = \frac{\pi}{64} D^4 . \quad (6)$$

Although stiffness measurements were conducted solely on the proximal region of the cupula, our morphological measurements provided a means to predict how flexural stiffness varies along

Table 1. *Flexural stiffness measurements*

N	Age (dpf)	L (mm)	D (μm)	h (μm)	l (mm)	$(EI)_{fiber}$ ($\times 10^{-11}$ N m^2)	m	$(EI)_{cup}$ ($\times 10^{-20}$ N m^2)
5	5	3.91	10.03	10.40	6.57	0.50	0.411	2.84
5	8	3.76	9.04	7.70	7.72	1.39	0.682	0.64
5	7	4.70	11.20	10.00	8.08	0.54	0.327	2.11
5	7	4.20	9.30	12.90	8.08	0.54	0.625	1.32
5	7	4.60	10.80	11.80	7.72	1.39	0.672	2.42
7	7	4.01	–	8.40	8.08	0.54	0.440	2.28
8	7	4.10	9.40	11.80	8.08	0.54	0.458	1.99
8	8	4.40	10.00	21.10	6.81	0.60	0.847	3.22
8	7	4.21	9.94	9.60	6.81	0.60	0.434	2.19
8	8	3.98	8.27	12.90	6.81	0.60	0.491	4.23
9	7	4.26	8.36	12.40	8.08	0.54	0.448	2.40
10	8	4.40	10.00	8.80	8.63	1.04	0.322	2.32
10	8	4.12	9.63	19.50	6.81	0.60	0.773	4.13
13	7	4.31	8.95	9.80	6.81	0.60	0.361	3.16
13	7	4.21	9.94	10.40	6.81	0.60	0.364	3.74

N, number of kinocilia; dpf, days post-fertilization; L, body length; D, neuromast base diameter; h, fiber height along cupula; l, fiber length; $(EI)_{fiber}$, flexural stiffness of fiber; m, slope of fiber displacements; $(EI)_{cup}$, flexural stiffness of cupula.

the length of the cupula. The contribution of the kinocilia to flexural stiffness at a particular height was calculated as the product of $(EI)_{kino}$ and the number of kinocilia (n) at that position. The stiffness provided by the cupular matrix along the cupular length was calculated as a product of Young's modulus of the matrix and the second moment of area as a function of height [Eqn 6, with D varying with height, i.e. $D(z)$]. Values for $D(z)$ and n were calculated for heights between measurements by linear interpolation.

Results

The flexural stiffness of individual superficial neuromasts was measured using the methods described above. Pressing a glass fiber against a cupula caused both structures to deflect. These deflections were recorded by tracking the position of the base (measured by optical strain gauge) and tip (measured with high-speed microscopy, Fig. 2) of the glass fiber (Fig. 3A). After filtering these data, we found the slope (m) describing the relationship between the displacement of the base (x_{base}) and tip (x_{tip}) of the glass fiber (Fig. 3B) in order to calculate the flexural stiffness of the cupula (using Eqn 3). This relationship was well approximated ($r^2 > 0.90$) by linear curve fits in all experiments. There were 15 successful experiments, all in separate individuals ($N=15$), and these results are provided in Table 1.

These measurements provided force–deflection curves from which an estimate of the forces used in our experiments could be inferred. In a representative experiment, a glass fiber pressed against a cupula with seven kinocilia at a height of 8.4 μm generated a deflection of ~2 μm (Fig. 3, Table 1). This deflection corresponded to a force applied against the cupula of ~0.35 nN (using Eqn 1). These values allow us to evaluate the implicit assumption in Eqn 1 that the cupula pivots little at its base. The base of the cupula experiences a moment generated by the applied force (8.4 μm$\times$0.35 nN=2.9$\times$10^{-15} N m), which is resisted by the hair bundles. These bundles may be modeled as torsion springs with a stiffness equal to that measured for canal neuromast hair cells [2.9$\times$10^{-14} N m rad^{-1} in the ruff,

Acerina cernua (van Netten and Kroese, 1987)]. The pivot angle at the base of the cupula may be calculated as the bending moment divided by the product of bundle stiffness and the number of hair cells (2.9$\times$10^{-15} N m/(2.9$\times$10^{-14} N m rad$^{-1}\times$7)= 0.014 rad). This calculation yields an angle that would permit a deflection at the tips of the kinocilia of 0.12 μm (0.014 rad$\times$8.4 μm), which is small (6%) relative to the measured deflection of 2 μm. Furthermore, this calculation assumes the hair bundles to be aligned with the neutral axis of the cupula and would predict much smaller deflections if it incorporated the actual distribution of hair bundles over the base of the cupula.

Flexural stiffness was significantly correlated with the number of hair cells (Fig. 4). The slope of this relationship was interpreted as being equivalent to the flexural stiffness of a single kinocilium (Eqn 5). We thereby determined a flexural stiffness of $(EI)_{kino}=2.4\times10^{-21}$ N m^2 for a kinocilium with 95% confidence intervals of $L_1=1.1\times10^{-21}$ N m^2 and $L_2=3.7\times10^{-21}$ N m^2. This range is slightly greater than the flexural stiffness of ATP-activated (demembranated) flagella (1.0×10^{-21} N m^2, Fig. 5) of sand dollar spermatozoa (*Clypeaster japonicus*) reported in the literature (Ishijima, 1994). The significance of this comparison is discussed below.

The cupular matrix made a small contribution to the flexural stiffness in the proximal region of the cupula. The matrix flexural stiffness is equal to the intercept of the linear regression (Eqn 5) for kinocilia number and flexural stiffness (Fig. 4). We found $(EI)_{matrix}=6.9\times10^{-21}$ N m^2 with an upper 95% confidence interval of $L_2=1.8\times10^{-20}$ N m^2 and lower interval of $L_1=-4.0\times10^{-21}$ N m^2. This negative value is physically impossible for a passive structure, so the lower limit was taken as zero ($L_1=0$). Using the mean value for $(EI)_{matrix}$ and the mean diameter of 8.88 μm for the cupula (see below) to calculate the second moment of area (Eqn 6; $I_{cup}=3.0\times10^{-22}$ m^4), Young's modulus for the matrix material was found to be 21 Pa. An upper limit of 53 Pa was calculated from the upper 95% confidence interval of our measurement for $(EI)_{matrix}$.
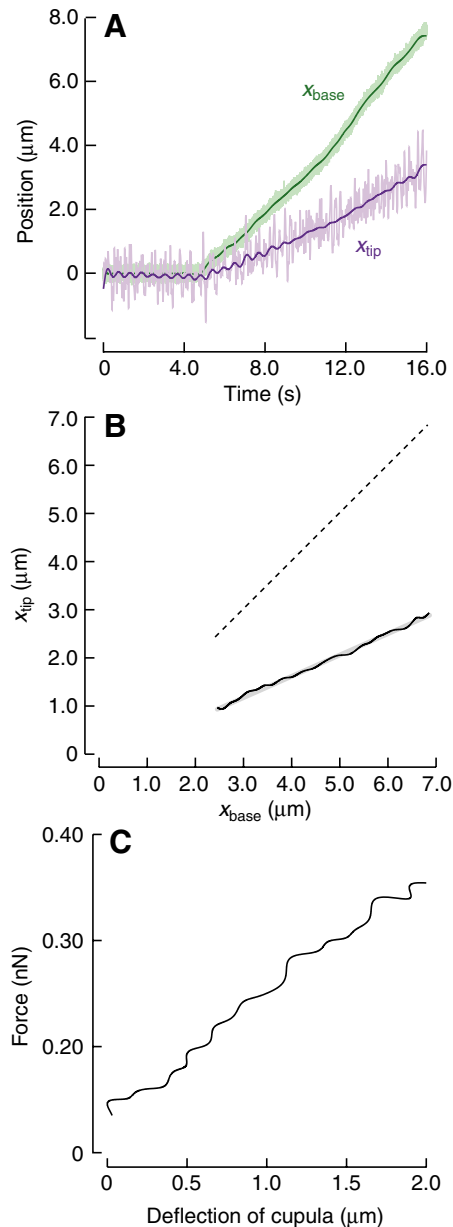
Fig. 3. A representative measurement of the flexural stiffness of a superficial neuromast. (A) Each stiffness measurement was calculated from measurements of the position of the fiber tip (x_{tip}, purple) and fiber base (x_{base}, green) of the glass fiber when pressed against a cupula. Noise was filtered from the raw data (light lines) to yield the position measurements used in the calculation (dark lines). (B) The filtered position data (solid black line) were used to calculate the stiffness of the cupula. The slope of a linear curve fitted to these data (gray line, $m=0.440$) yielded a flexural stiffness for the cupula [$(EI)_{cup}=2.28\times10^{-20}$ N m^2] using Eqn 3. A slope equal to unity (dashed line, $m=1$) represents the relationship predicted for a completely compliant neuromast. (C) The positional changes from B provide the basis for the calculation of the deflection of the cupulae and the force exerted by the fiber to cause that deflection.

We estimated that the flexural stiffness of a superficial neuromast decreases along its height (Fig. 6). At the base of an average neuromast, the relatively large diameter (8.88 μm) of
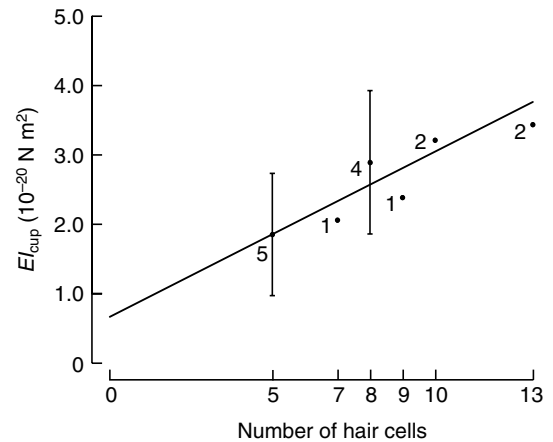

Fig. 4. The relationship between the number of hair cells (each with one kinocilium) and the flexural stiffness of the cupula [$(EI)_{cup}$]. Mean values (±1s.d., numbers next to points denote the sample size for each point) are shown for neuromasts of a variable number of hair cells. The trend line represents a significant ($P<0.015$) weighted linear regression that suggests that most of the variation ($r^2=0.81$) in flexural stiffness is related to the number of hair cells. This trend was predicted by our hypothesis (Eqn 5), which interprets the slope of this line (2.4×10^{-21} N m^2) as the stiffness generated by a single kinocilium.

the cupular matrix is predicted to generate a flexural stiffness of 0.6×10^{-20} N m^2 (assuming $E_{matrix}=21$ Pa). This value is about one-fifth the total stiffness [$(EI)_{cup}=3.3\times10^{-20}$ N m^2] of the proximal region (assuming 11 kinocilia and $(EI)_{kino}=2.4\times10^{-21}$ N m^2). Tapering in the diameter of the cupula leads to a decrease from a mean diameter of 8.88 μm at its base to 7.2 μm at a height of 16 μm, and 5.5 μm at a height of 32.0 μm (Fig. 6C). This causes a gradual reduction in stiffness generated by the matrix (Fig. 6E). Kinocilia exhibited a gradual decrease in number from a mean value of 11 at the base, to eight at a height of 16 μm, while being completely absent beyond a height of 24 μm. These reductions in the number of kinocilia strongly influence cupular flexural stiffness (Fig. 6E). Therefore, flexural stiffness is predicted to vary solely with the second moment of area of the matrix in the cupular tip region. Together, the reduction in the number of kinocilia and cupular diameter with increasing height result in a decrease of superficial cupular flexural stiffness at the proximal region (3.3×10^{-20} N m^2) to less than an order of magnitude lower (0.2×10^{-20} N m^2) at the tip region (Fig. 6E).

Discussion

Our measurements of cupular flexural stiffness provide a basis for understanding the micromechanics of superficial neuromasts. According to our results, kinocilia dominate the flexural stiffness of the proximal region. The cupular matrix surrounds and extends beyond the kinocilia, thereby forming a highly flexible tip. This suggests that a superficial cupula functions as a two-part beam with mechanical properties that are largely determined by the height and number of kinocilia.

The flexural stiffness of kinocilia

Kinocilia are similar to cilia and eukaryotic flagella in their ultrastructure. They possess a 9+2 arrangement of microtubules
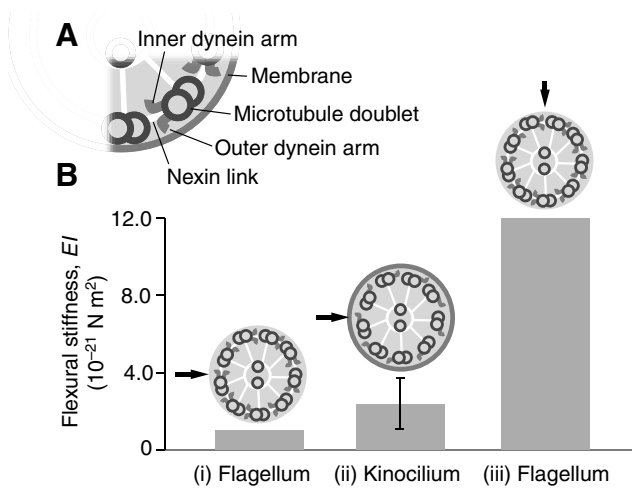
Fig. 5. Measurement of flexural stiffness (*EI*) of a kinocilium compared with that of a flagellum. (A) The schematic illustration of a portion of an axoneme shows major features of the ultrastructure of flagella and kinocilia. (B) Arrows directed at the axonemes above each bar indicate the direction of loading for each measurement of stiffness. Flagellar stiffness was measured in demembranated sperm of the sand dollar (*Clypeaster japonicus*) activated by ATP (Ishijima and Hiramoto, 1994). (i) The stiffness of a flagellum when loaded along its beating plane is shown in comparison to measurements of stiffness for (ii) a kinocilium from the present study (error flags denote 95% confidence intervals) and the stiffness of (iii) a flagellum when loaded perpendicular to the beating plane.

(Fawcett, 1961; Flock and Duvall, 1965) with radial spokes and outer dynein arms [Fig. 5A,B(ii)]. However, kinocilia lack nexin links and inner dynein arms [Fig. 5B(i)], which may preclude motility (Kikuchi et al., 1989). Although their ability to generate force has not been ruled out (Ross et al., 1987), kinocilia are generally regarded as passive transmitters of

deflections that are transduced by channels in the stereocilia (Hudspeth and Jacobs, 1979).

Given their similarities in ultrastructure, it is informative to compare our measurements of flexural stiffness in kinocilia with that in cilia and flagella. Our measurements for the flexural stiffness of kinocilia (1.1×10^{-21} to 3.7×10^{-21} N m^2) are about 100 times lower than the direct measurements (2×10^{-19} to 3×10^{-19} N m^2) from gill cilia in a clam (*Mytilus edulis*) by Baba (Baba, 1972). However, Okuno and Hiramoto (Okuno and Hiramoto, 1979) could not replicate these results in sea urchin (*Hemicentrotus pulcherrimus*) flagella, which showed substantially lower flexural stiffness ($\sim 1 \times 10^{-20}$ N m^2). When treated with 10 mmol l^{-1} ATP, demembranated flagella became an order of magnitude less flexible ($\sim 1 \times 10^{-21}$ N m^2), presumably because ATP causes dynein to detach from the microtubules within the axoneme (Okuno and Hiramoto, 1979). This measure of stiffness was verified in sand dollar (*Clypeaster japnicus*) spermatozoa that were loaded hydrodynamically (Ishijima and Hiramoto, 1994). We found this value to be slightly, but significantly, less than our measurements for the flexural stiffness of a kinocilium [Fig. 5B(ii)]. The greater stiffness of kinocilia is probably a consequence of greater spacing between their microtubule doublets [178 nm between outer edges (Flock and Duvall, 1965)] than in flagella (158 nm) (Brokaw, 1989).

The structural and mechanical similarities between kinocilia and flagella raise the potential that kinocilia are polarized in their mechanics. The present study measured flexural stiffness in the kinocilia of the P8 neuromast (Fig. 1) by applying force in the anterio-posterior direction. It is in this direction that the neuromast is sensitive, due to its arrangement of stereocilia (Lopez-Schier et al., 2004). This direction of loading is perpendicular to the axis of the central pair of microtubules within the kinocilium [Fig. 5B(ii)] (Flock and Duvall, 1965). Using the central pair for alignment, the kinocilia in the present
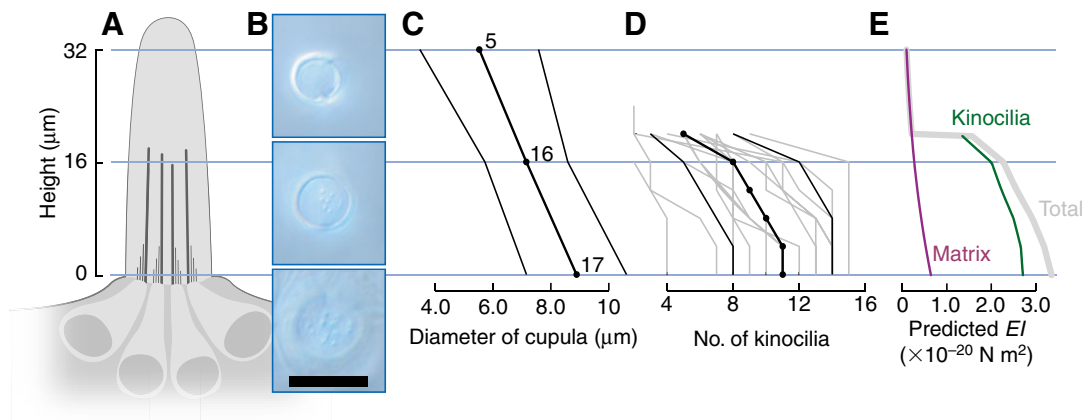

Fig. 6. Variation in morphology and mechanics along the height of the cupula. (A) A schematic illustration showing the major morphological differences along the height of a cupula. (B) Photographs of cross-sections of a typical neuromast at three different heights. (C) The diameter of the cupula decreases with height, as shown by mean values (points and heavy line, ±1s.d. shown by thin lines, numbers indicate sample size). (D) The number of kinocilia in a cross-section decreases with height. Data for individual cupulae (gray lines) and mean values (points and heavy line, ±1s.d. shown by thin lines) are shown. (E) The mean values of the morphological data in D, along with our measurements of flexural stiffness (*EI*, Fig. 4), provide the basis for calculations of cupular flexural stiffness *versus* height. The total flexural stiffness of the cupula (gray line) is dominated by the stiffness provided by the kinocilia (green line) in the proximal region. The stiffness of the cupular matrix provides a substantially more flexible structure in the distal region, where kinocilia are absent.
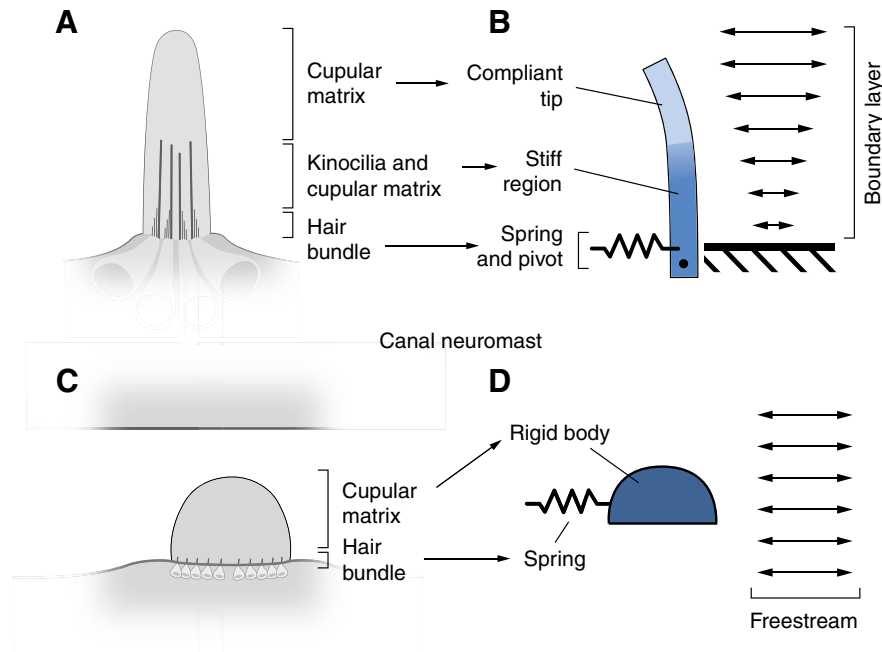
Fig. 7. Proposed model for the mechanics of a superficial neuromast compared with the mechanics of a canal neuromast. (A) The major morphological features of a superficial neuromast each have a functional analog. (B) The proposed model consists of a flexible two-part beam that is driven by a boundary layer of water flow and coupled to a linear pivotal spring at its base. The presence of kinocilia causes the proximal part of this beam to be substantially stiffer than the distal part, which consists solely of matrix material. The morphology and mechanics of superficial neuromasts is contrasted with (C,D) the model for a canal neuromast (van Netten and Kroese, 1987). (C) The same major anatomical features of a superficial neuromast are present in the canal neuromast, but (D) kinocilia do not play a functional role that is distinct from the hair bundles, which collectively function as a linear spring. Furthermore, the cupula is modeled as a rigid hemispherical body that is coupled to the hair bundles. The freestream flow within the canal is not greatly influenced by boundary layer dynamics for the frequencies to which these neuromasts are sensitive (van Netten, 2006) and may therefore be modeled as a uniform freestream.

study were loaded in the same direction as the beating plane of a flagellum [Fig. 5B(i)]. Ishijima and Hiramoto (Ishijima and Hiramoto, 1994) found the passive stiffness of flagella along the beating plane to be lower than when they were loaded perpendicular to this plane [1.2×10^{-20} N m^2, Fig. 5B(iii)] by a factor of 12. If one assumes similar polarity, then kinocilia would be predicted to be more than an order of magnitude more flexible in the direction in which the hair cells sense flow (anterio-posterior, in this case) than in the perpendicular direction (dorso-ventral).

Young's modulus of the cupular matrix

Prior studies have suggested that the cupular matrix possesses a biochemical composition that is grossly similar to the mesoglea of cnidarians. Like mesoglea, the cupula is composed of a well-hydrated neutral glycosaminoglycan gel (Sato, 1962; Thomopolous, 1958). Mesoglea commonly contains protein fibrils composed of collagen, collagen-like and fibrillin-like molecules (Chapman, 1953; Grimstone et al., 1958; Gosline, 1971; Megill et al., 2005). The cupula includes extracellular fibrils of unknown composition in the canal neuromasts (Jielof et al., 1952; Flock, 1965b; Munz, 1979; Kelly and van Netten, 1991) and the superficial neuromasts of some species [e.g. *Fudulus heteroclitius* (Denny, 1937)], but not others [e.g. *Sarotherodon niloticus* (Munz, 1979)]. Such fibrils were not found in the superficial neuromasts of embryonic zebrafish previously (Munz, 1979) and were not observed in larvae with

polarized or differential interference contrast microscopy in the present study.

The relatively high compliance of the zebrafish cupula appears to be related its lack of fibrils. Its Young's modulus (~21 Pa) is more than two orders of magnitude less than that of blind cavefish (~8 kPa in *Astyanax fasciaus*) (Peleshanko et al., 2007), which appear to possess fibrils (in *Astyanax hubbsi*) (Teyke, 1990). An even greater range of Young's modulus is found in mesoglea. For example, the high fibril density of sea anemone (*Anthopleura xanthogrammica*) mesoglea has a Young's modulus (~100 kPa) (Koehl, 1977) that is four orders of magnitude greater than that of mesoglea lacking these fibrils (e.g. *Polycorchis penicillatus*) (Megill et al., 2005). Mesoglea lacking fibrils from the bell of some hydromedusae has an estimated Young's modulus (~50 Pa) (Megill et al., 2005) that is similar to what we have found for the cupula of zebrafish larvae. This is not surprising given the similar molecular composition of mesoglea and the cupular matrix.

It is unclear whether the viscoelasticity of the cupular matrix influences its function. The viscoelastic properties of mesoglea largely determine how sea anemones respond to hydrodynamic loads over different timescales (Koehl, 1977) and dictate the resilience of the bell of swimming jellyfish (DeMont and Gosline, 1988). It therefore is conceivable that the viscous component of the cupula matrix (Peleshanko et al., 2007) could act to filter high-frequency stimuli. Alternatively, the dominance of kinocilia in the proximal region (Fig. 6) may

cause the cupula to respond elastically to hydrodynamic loads. Given the quasi-static nature of the present experiments, further investigation will be necessary to resolve the role of structural viscosity in the mechanics of superficial neuromasts.

A model for superficial neuromast mechanics

Our results suggest a model for the structural mechanics of superficial neuromasts (Fig. 7A,B). According to this model, the cupula behaves as a beam that is anchored to hair bundles, is stiff in its proximal region, and is compliant at its distal tip. The juncture at the base of the cupula behaves as a pivot that is coupled to hair bundles that act as a spring. The proximal region of the cupula has a flexural stiffness that is proportional to the number of kinocilia (Fig. 4). This stiff region extends to the height of the kinocilia, with the remainder of the cupula height providing a compliant tip. The cupula deflects when excited by flow that is governed by boundary layer hydrodynamics over the surface of the body (Jielof et al., 1952; Kuiper, 1967; Hassan, 1985; Kalmijn, 1988; Teyke, 1988; Dinklo, 2005).

This model suggests that the sensitivity of a superficial neuromast largely depends on its morphology. The hair cells within a neuromast generate transducer potentials that are proportional to the deflection of the kinocilia at low amplitudes (Flock, 1965a). Therefore, morphological properties that increase flexural stiffness serve to reduce the sensitivity of the neuromast by decreasing deflection. For example, a greater number of hair cells within a neuromast provides more kinocilia that stiffen the cupula and reduce sensitivity. Similarly, a cupula of greater diameter will have a larger second moment of area that acts to reduce deflection. However, these features may also promote sensitivity. Although a greater number of hair cells will stiffen the cupula, the neurobiological sensitivity of the neuromast will increase because there are more sensory cells. A larger cupula diameter increases flexural stiffness, but also provides a greater area for fluid forces to cause greater deflection. Therefore, trade-offs exist in the design of neuromasts that suggest the possibility that an optimal combination of morphological parameters could maximize the sensitivity of an individual neuromast. The design of neuromast arrays may alternatively benefit from a variation in morphology that creates a variety of frequency responses and sensitivities to facilitate range fractionation.

Our superficial neuromast model contrasts the micromechanics of canal neuromasts (Fig. 7C,D). Most strikingly, the structural dynamics of the cupula do not play an important role in the function of a canal neuromast. van Netten and Kroese (van Netten and Kroese, 1987) demonstrated that the cupula slides along the sensory epithelium as a rigid body. Therefore, canal neuromasts have been modeled as a rigid hemisphere that is coupled to hair bundles that function as a linear spring. This structure is driven by a uniform flow field within the canal (van Netten and Kroese, 1989) at the frequencies to which a canal neuromast is sensitive (>20 Hz). This flow varies in proportion to the difference in pressure between its pores (Denton and Gray, 1983; van Netten, 2006). In contrast, superficial neuromasts are directly exposed to a stimulus field and are sensitive to low frequency stimuli (<80 Hz) (Kroese and Schellart, 1992). At these frequencies, the boundary layer generates a spatial gradient in flow at the body's

surface (Jielof et al., 1952; Kuiper, 1967; Hassan, 1985; Kalmijn, 1988; Teyke, 1988; Dinklo, 2005).

The role of structural dynamics in the frequency response of a neuromast is inextricably linked to the hydrodynamics that excite the system. The fluid forces generated by a stimulus depend on the speed and acceleration of flow relative to the motion of the cupula. This motion and, consequently, the fluid forces depend on the structural properties of the neuromast. This is illustrated mathematically by the canal neuromast model. The equations describing the hydrodynamics of the canal cupula cannot be solved without considering the stiffness of the hair bundles (van Netten and Kroese, 1989; van Netten and Kroese, 1987). Similarly, formulating a prediction for the frequency response of a superficial neuromast will require consideration of the fluid–structure interaction between the cupula and surrounding flow.

References

Alexandre, D. and Ghysen, A. (1999). Somatotopy of the lateral line projection in larval zebrafish. *Proc. Natl. Acad. Sci. USA* **96**, 7558-7562.
Appelbaum, S. and Riehl, R. (1997). Scanning electron microscopic observations of the chemo- and mechanoreceptors of carp larvae (*Cyprinus carpio*) and their relationship to early behavior. *Aquat. Living Resour.* **10**, 1-12.
Baba, S. A. (1972). Flexural rigidity and elastic-constant of cilia. *J. Exp. Biol.* **56**, 459-467.
Blaxter, J. H. (1984). Cupular growth in herring neuromasts. *J. Mar. Biol. Assoc. U. K.* **64**, 935-938.
Blaxter, J. H. S. and Fuiman, L. A. (1989). Function of the free neuromasts of marine teleost larvae. In *The Mechanosensory Lateral Line: Neurobiology and Evolution* (ed. S. Coombs, P. Gorner and H. Munz), pp. 481-499. New York: Springer-Verlag.
Brand, M., Granato, M. and Nuesslein-Volhard, C. (2002). Keeping and raising zebrafish. In *Zebrafish* (ed. C. Nusslein-Volhard and R. Dahm), pp. 7-38. Oxford: Oxford University Press.
Brokaw, C. J. (1989). Direct measurements of sliding between outer doublet microtubules in swimming sperm flagella. *Science* **243**, 1593-1596.
Cahn, P. H. and Shaw, E. (1962). The first demonstration of lateral line cupulae in the mugiliformes. *Copeia* **1962**, 109-114.
Chapman, G. (1953). Studies of the mesoglea of coelenterates. I. Histology and chemical properties. *Q. J. Microsc. Sci.* **94**, 155-176.
Corey, D. P., Garcia-Anoveros, J., Holt, J. R., Kwan, K. Y., Lin, S. Y., Vollrath, M. A., Amalfitano, A., Cheung, E. L. M., Derfler, B. H., Duggan, A. et al. (2004). TRPA1 is a candidate for the mechanosensitive transduction channel of vertebrate hair cells. *Nature* **432**, 723-730.
DeMont, M. E. and Gosline, J. M. (1988). Mechanics of jet propulsion in the hydromedusan jellyfish, *Polyorchis penicillatus*. I. Mechanical properties of the locomotor structure. *J. Exp. Biol.* **134**, 313-332.
Denny, M. (1937). The lateral-line system of the teleost *Fundulud heteroclitus*. *J. Comp. Neurol.* **68**, 49-65.
Denton, E. J. and Gray, J. (1983). Mechanical factors in the excitation of clupeid lateral lines. *Proc. R. Soc. Lond. B Biol. Sci.* **218**, 1-26.
Dijkgraaf, S. (1952). Bau und Funktionen der Seitenorgane und dcs Ohrlabyrinths bei Fischen. *Experientia* **8**, 205-216.
Dinklo, T. (2005). Mechano- and electrophysiological studies on cochlear hair cells and superficial lateral line cupulae. PhD thesis, University of Groningen, The Netherlands.
Fan, Z., Chen, J., Zou, J., Bullen, D., Liu, C. and Delcomyn, F. (2002). Design and fabrication of artificial lateral line flow sensors. *J. Micromech. Microeng.* **12**, 655-661.
Fawcett, D. W. (1961). Cilia and Flagella. In *The Cell* (ed. J. Brachet and A. E. Mirsky), pp. 217-287. New York: Academic Press.
Flock, A. (1965a). Transducing mechanisms in lateral line canal organ receptors. *Cold Spring Harb. Symp. Quant. Biol.* **30**, 133-145.

Flock, A. (1965b). Electron microscopic and electrophysiological studies on the lateral line canal organ. *Acta Otolaryngol. Suppl.* **199**, 1-90.

Flock, A. and Duvall, A. J. (1965). The ultrastructure of the kinocilium of the sensory cells in the inner ear and lateral line organs. *J. Cell Biol.* **25**, 1-8.

Gere, J. M. (2001). *Mechanics of Materials*. Cheltenham: Nelson Thornes.

Gosline, J. M. (1971). Connective tissue mechanics of *Metridium senile*. II Visco-elastic properties and macromolecular model. *J. Exp. Biol.* **55**, 775-795.

Grimstone, A. V., Horne, R. N., Pantin, C. F. A. and Robson, E. A. (1958). The fine structure of the mesenteries of the sea anemone *Metridium senile*. *Q. J. Microsc. Sci.* **99**, 523-540.

Hassan, E. S. (1985). Mathematical analysis of the stimulus of the lateral line organ. *Biol. Cybern.* **52**, 23-36.

Hassan, E. S. (1986). On the discrimination of spatial intervals by the blind cave fish (*Anoptichthys jordani*). *J. Comp. Physiol. A* **159**, 701-710.

Hudspeth, A. J. and Jacobs, R. (1979). Stereocilia mediate transduction in vertebrate hair cells. *Proc. Natl. Acad. Sci. USA* **76**, 1506-1509.

Ishijima, S. and Hiramoto, Y. (1994). Flexural rigidity of echinoderm sperm flagella. *Cell Struct. Funct.* **19**, 349-362.

Jielof, R., Spoor, A. and de Vries, H. (1952). The microphonic activity of the lateral line. *J. Physiol.* **116**, 137-157.

Kalmijn, A. J. (1988). Hydrodynamic and acoustic field detection. In *Sensory Biology of Aquatic Animals* (ed. J. Atema, R. R. Fay, A. N. Popper and W. N. Tavolga), pp. 83-130. New York: Springer-Verlag.

Kelly, J. P. and van Netten, S. M. (1991). Topology and mechanics of the cupula in the fish lateral line. Variations of cupular structure and composition in three dimensions. *J. Morphol.* **207**, 23-36.

Kikuchi, T., Takasaka, T., Tonosaki, A. and Watanabe, H. (1989). Fine structure of guinea pig vestibular kinocilium. *Acta Otolaryngol.* **108**, 26-30.

Koehl, M. A. R. (1977). Mechanical diversity of connective tissue of the body wall of sea anemones. *J. Exp. Biol.* **69**, 107-125.

Kroese, A. B. A. and Schellart, N. A. M. (1992). Velocity and acceleration-sensitive units in the trunk lateral line of the trout. *J. Neurophysiol.* **68**, 2212-2221.

Kroese, A. B. A. and van Netten, S. M. (1989). Sensory transduction in lateral line hair cells. In *The Mechanosensory Lateral Line: Neurobiology and Evolution* (ed. S. Coombs, P. Gorner and H. Munz), pp. 265-284. New York: Springer-Verlag.

Kuiper, J. W. (1967). Frequency characteristics and functional significance of the lateral line organ. In *Lateral Line Detectors* (ed. P. H. Cahn), pp. 105-121. Bloomington: Indiana University Press.

Liu, K. S. and Fetcho, J. R. (1999). Laser ablations reveal functional relationships of segmental hindbrain neurons in zebrafish. *Neuron* **23**, 325-335.

Lopez-Schier, H., Starr, C. J., Kappler, J. A., Kollmar, R. and Hudspeth, A. J. (2004). Directional cell migration establishes the axes of planar polarity in the posterior lateral-line organ of the zebrafish. *Dev. Cell* **7**, 401-412.

Megill, W. M., Gosline, J. M. and Blake, R. W. (2005). The modulus of elasticity of fibrillin-containing elastic fibers in the mesoglea of the hydromedusa *Polyorchis penicillatus*. *J. Exp. Biol.* **208**, 3819-3834.

Metcalfe, W. K., Kimmel, C. B. and Schabtach, E. (1985). Anatomy of the posterior lateral line system in young larvae of the zebrafish. *J. Comp. Neurol.* **233**, 377-389.

Montgomery, J. C., Baker, C. F. and Carton, A. G. (1997). The lateral line can mediate rheotaxis in fish. *Nature* **389**, 960-963.

Munz, H. (1979). Morphology and innervation of the lateral line system in *Sarotherodon niloticus* (L.) (Cichlidae, Teleostei). *Zoomorphologie* **93**, 73-86.

Munz, H. (1989). Functional organization of the lateral line periphery. In *The Mechanosensory Lateral Line* (ed. S. Coombs, P. Gorner and H. Munz), pp. 285-298. Berlin: Springer-Verlag.

Nicolson, T., Rusch, A., Friedrich, R. W., Granato, M., Ruppersberg, J. P. and Nusslein-Volhard, C. (1998). Genetic analysis of vertebrate sensory hair cell mechanosensation: the zebrafish circler mutants. *Neuron* **20**, 271-283.

Northcutt, R. G. (1989). The phylogenetic distribution and innervation of craniate mechanoreceptive lateral lines. In *The Mechanosensory Lateral Line* (ed. S. Coombs, P. Gorner and H. Munz), pp. 17-78. New York: Springer-Verlag.

Okuno, M. and Hiramoto, Y. (1979). Direct measurements of the stiffness of echinoderm flagella. *J. Exp. Biol.* **79**, 235-243.

Peleshanko, S., Julian, M. D., Ornatska, M., McConney, M. E., LeMieux, M. C., Chen, N., Tucker, C., Yang, Y., Liu, C., Humphrey, J. A. C. and Tsukruk, V. V. (2007). Hydrogel-encapsulated microfabricated haircell mimicking fish cupulae neuromast. *Adv. Mat.* **19**, 2903-2909.

Poling, K. R. and Fuiman, L. A. (1997). Sensory development and concurrent behavioral changes in Atlantic croaker larvae. *J. Fish Biol.* **51**, 402-421.

Quinn, G. P. and Keough, M. J. (2002). *Experimental Design and Data Analysis for Biologists*. Cambridge: Cambridge University Press.

Raible, D. W. and Kruse, G. J. (2000). Organization of the lateral line system in embryonic zebrafish. *J. Comp. Neurol.* **421**, 189-198.

Ross, M. D., Komorowski, T. E., Rogers, C. M., Pote, K. G. and Donovan, K. M. (1987). Macular suprastructure, stereociliary bonding and kinociliary/stereociliary coupling in rat utricular macula. *Acta Otolaryngol.* **104**, 56-65.

Sato, M. (1962). Studies on the pit organs of fishes V. The structure and polysaccharide histochemistry of the cupula pit organ. *Annot. Zool. Jpn.* **35**, 80-88.

Satou, M., Takeuchi, H. A., Tanabe, M., Kitamura, S., Okumoto, N., Iwata, M. and Nishii, J. (1994). Behavioral and electrophysiological evidences that the lateral-line is involved in the inter-sexual vibrational communication of the hime salmon (landlocked red salmon, *Oncorhynchus-nerka*). *J. Comp. Physiol. A* **174**, 539-549.

Schulze, F. E. (1861). Uber die Nervenendigung in den sogenannten Schleimkanalen der Fische und uber entsprechende Organe der durch Kiemen athmenden Amphibien. *Arch. Anat. Physiol. Lpz.* 759-769.

Sidi, S., Friedrich, R. W. and Nicolson, T. (2003). NompC TRP channel required for vertebrate sensory hair cell mechanotransduction. *Science* **301**, 96-99.

Taylor, J. R. (1982). *An Introduction to Error Analysis: The Study of Uncertainties in Physical Measurements*. Mill Valley, CA: University Science Books.

Teyke, T. (1988). Flow field, swimming velocity, and boundary layer: parameters which affect the stimulus for the lateral line organ in blind fish. *J. Comp. Physiol. A* **163**, 53-61.

Teyke, T. (1990). Morphological differences in neuromasts of the blind cave fish *astyanax hubbsi* and the sighted river fish *astyanax mexicanus*. *Brain Behav. Evol.* **35**, 23-30.

Thomopolous, A. (1958). Sur la ligne latérale des Téléostiéns. II. La cupule et les neuromasts chez des embryons et des larves planctoniques d'espéces marines. *Bull. Soc. Zool. Fr.* **82**, 437.

Timoshenko, S. P. (1983). *History of Strength of Materials*. New York: Dover.

van Netten, S. M. (2006). Hydrodynamic detection by cupulae in a lateral line canal: functional relations between physics and physiology. *Biol. Cybern.* **94**, 67-85.

van Netten, S. M. and Kroese, A. B. A. (1987). Laser interferometric measurements on the dynamic behavior of the cupula in the fish lateral line. *Hear. Res.* **29**, 55-62.

van Netten, S. M. and Kroese, A. B. A. (1989). Dynamic behavior and micromechanical properties of the cupula. In *The Mechanosensory Lateral Line: Neurobiology and Evolution* (ed. S. Coombs, P. Gorner and H. Munz), pp. 247-263. New York: Springer-Verlag.

Wainwright, S. A., Biggs, W. D., Currey, J. D. and Gosline, J. M. (1976). *Mechanical Design in Organisms*. Princeton, NJ: Princeton University Press.

Webb, J. F. (1989). Neuromast morphology and lateral line trunk canal ontogeny in 2 species of cichlids – an SEM study. *J. Morphol.* **202**, 53-68.

Webb, J. F. (1990). Ontogeny and phylogeny of the trunk lateral line system in cichlid fishes. *J. Zool.* **221**, 405-418.

Webb, J. F. and Shirey, J. E. (2003). Postembryonic development of the cranial lateral line canals and neuromasts in zebrafish. *Dev. Dyn.* **228**, 370-385.

Westerfield, M. (1995). *The Zebrafish Book: A Guide for the Laboratory Use of Zebrafish, Brachydanio rerio*. Eugene, OR: University of Oregon Press.